PAPER

Structural properties of iron-phosphate glasses: spectroscopic studies and *ab initio* simulations

Pawel Stoch,*[a] Wojciech Szczerba,[b] Wiktor Bodnar,[c] Malgorzata Ciecinska,[a] Agata Stoch[d] and Eberhard Burkel[c]

Vitrification is the most effective method for the immobilization of hazardous waste by incorporating toxic elements into a glass structure. Iron phosphate glasses are presently being considered as matrices for the storage of radioactive waste, even of those which cannot be vitrified using conventional borosilicate waste glass. In this study, a structural model of $60P_2O_5-40Fe_2O_3$ glass is proposed. The model is based on the crystal structure of $FePO_4$ which is composed of $[FeO_4][PO_4]$ tetrahedral rings. The rings are optimized using the DFT method and the obtained theoretical FTIR and Raman spectra are being compared with their experimental counterparts. Moreover, the proposed model is in very good agreement with X-ray absorption fine structure spectroscopy (XANES/EXAFS) and Mössbauer spectro-scopy measurements. According to the calculations the Fe^{3+} is in tetrahedral and five-fold coordination. The maximal predicted load of waste constituents into the glass without rebuilding of the structure is 30 mol%. Below this content, waste constituents balance the charge of $[FeO_4]^-$ tetrahedra which leads to their strong bonding to the glass resulting in an increase of the chemical durability, transformation and melting temperatures and density.

1 Introduction

Vitrification is the most effective method for the immobilization of hazardous waste. Toxic elements are incorporated into the glass structure and stay bonded to it. For many years borosilicate glasses have been of common use in the nuclear waste immo-bilization procedure. Lately the $Fe_2O_3-P_2O_5$ glasses have been of great interest, for scientific reasons and because they are con-sidered as high capacity matrices for storage of radioactive waste.[1,2] The worldwide used borosilicate glasses for nuclear waste vitrification are not suitable for immobilization of waste with a high content of molybdenum, chromium or salts because of the low solubility of these compounds in the glass. Therefore, it is necessary to look for an alternative vitrification matrix. The next choice is the phosphate glass. However, most phosphate glasses have a low chemical durability,[3] but iron as a glass compo-nent significantly increases it. The $60P_2O_5-40Fe_2O_3$ (Fe/P = 0.67) glass has the highest chemical durability among others. All of them

have an O/P ratio of over 3 and are classified as polyphosphate glasses.[4] There are indications that iron strengthens the chemical bonds in the glass structure making their properties comparable or even better than those of borosilicate glasses.[1,2]

Besides their excellent chemical durability, iron phosphate glasses have the melting temperature of about 100–200 K lower than borosilicate glass and also due to lower viscosity of the melts their homogenization time is about 1.5–3 hours shorter.[5] It is why they can be suitable for vitrifying waste containing significant quantities of volatile elements such as Cs. Moreover, iron phosphate glasses exhibit particularly high thermal stability in terms of the low crystallization ability and can be produced in large quantities without the danger of crystallization of the matrix. Nevertheless, glassy materials with crystalline particulate inclusions were also obtained in particular cases depending on the composition and heating schedule.[1]

Iron phosphate glasses are now considered for the vitrifica-tion of waste containing a relatively high concentration of actinide elements, a high concentration of sodium, caesium sulphate and chloride, chloride waste from pyrochemical repro-cessing of Pu metal and waste containing various metals, radioactive ceramics, polymers or carbon.[1,6]

The structure of phosphate glasses can be described in a convenient way using the Q^i notation. The Q^i represents the phosphate tetrahedra, where *i* represents the number of neigh-bouring P-tetrahedra linked by common bridging oxygens.[4,7] Single component P_2O_5 glass is built of only Q^3 tetrahedra

[a] *Faculty of Material Science and Ceramics, AGH-University of Science and Technology, 30 Mickiewicza Av, 30349 Krakow, Poland.*
E-mail: pstoch@agh.edu.pl; Fax: +48 12633 4630; Tel: +48 12617 2504
[b] *BAM Federal Institute for Materials Research and Testing, Unter den Eichen 87, 12205 Berlin, Germany*
[c] *Institute of Physics, University of Rostock, August-Bebel-Str. 55, 18055 Rostock, Germany*
[d] *Institute of Electron Technology Krakow Division, Zablocie 39, 30701 Krakow, Poland*

This journal is © the Owner Societies 2014

Phys. Chem. Chem. Phys., 2014, **16**, 19917–19927 | 19917

which have three bridging oxygens and one non-bridging oxygen atom (P=O). Phosphate glasses can be described as a range of structures, from a three dimensional cross-linked network of Q^3 tetrahedra to polymer-like metaphosphate chains of Q^2 tetrahedra to glasses based on small pyro-(Q^1) and orthophosphate (Q^0) anions. The Q^i notation assumes only one type of network forming cations. In the case of iron-phosphate glasses there is a possibility that, similar to that in silicate glasses, Fe^{3+} could be a network former or a network modifier. Therefore the Q_n notation instead of Q^i is used in the present paper. The Q_n notation expresses the concentration of bridging oxygens per tetrahedron by varying the value of n. A tetrahedron fully linked into the network *via* four bridging oxygens is designated as a Q_4 unit, while an isolated tetrahedron with no bridging oxygens is designated as a Q_0 unit. The value of n is thus equal to the number of bridging oxygens in a given tetrahedron.[8]

The local structure of iron is complicated by the fact that depending on conditions of synthesis, the glass may contain variable amounts of Fe^{2+} ions. It leads to extremely complex crystallography of the iron phosphate system which is composed of over 20 different crystalline phases in which iron can be present in both valence states and coordination numbers to oxygen from 4 to 6. In the case of iron phosphate glasses the structural analogue of SiO_4 tetrahedra (a main building block of silicate glasses) is $FePO_4$ which is characteristic of a similar phase transition from α-quartz to β-quartz at 980 K with alternate corner sharing of both $[FeO_4]^-$ and $[PO_4]^+$ tetrahedra. For glasses which possess excess of P_2O_5 some possible structural models were already proposed. The first model was proposed by Wedgwood.[9] Here, the glass structure is built of three different units $[FeO_4]^-$ and $[PO_4]^+$ tetrahedra sharing all four vertices like in α-$FePO_4$ and O=PO_3 units, which are PO_4 tetrahedra with one terminal double bonded oxygen and three vertices sharing single bonded oxygen atoms. In this model all of the Fe^{2+} cations are present as network modifiers in octahedral coordination. The next model was proposed by Marasinghe *et al.*[10] and is based on the crystal structure of $Fe_3(P_2O_7)_2$ in which one Fe^{2+} ion is present in trigonal prismatic coordination and two Fe^{3+} ions in octahedral coordination. On the other hand, glasses with high Fe_2O_3 content exhibit short range antiferromagnetic ordering at low temperatures, very similar to α-quartz $FePO_4$, which is hence the first structural model. Wright *et al.*[11] proposed a nanoheterogenous model comprising regions with alternating $[FeO_4]^-$ and $[PO_4]^+$ corner sharing tetrahedra, together with separate regions in which the glass contains both tetrahedral Fe^{3+} and octahedral Fe^{2+}/Fe^{3+} cations.

The magnetic structure of these glasses is quite complex and confirms the presence of speromagnetic ordering.[9,12,13] The magnetic correlation function obtained by the neutron scattering method shows the existence of negative peaks at 3.7 Å and 5.8–5.9 Å, which suggests that the average magnetic moment of the atoms at this distance tends to be anti-parallel and the broad positive effect appears at 8–10 Å distance.[9,10]

It is worth mentioning that in iron-phosphate glasses part of iron is always in the ferrous state with its amount depending on the synthesis conditions from about 10 to even 100%. On the other hand, during studies on immobilization of caesium, glasses with almost only ferric iron but with some Cs_2O content were obtained. The structure of these glasses does not change with Cs_2O content up to about 22 mol%, but above this threshold some structural changes are observed.[14,15] Analogously, investigations on immobilization of Na_2SO_4 in similar glasses showed an increase in the stability of the glass structure up to about 30 mol% and rebuilding it for higher contents of Na_2O.[16]

Motivated by the aforementioned studies, a structural model of the 60P_2O_5–40Fe_2O_3 glass is presented. The model was optimised using the DFT method. The calculated theoretical FTIR and Raman spectra were compared with the experimental results. Moreover, the proposed model was evaluated applying EXAFS/XANES and Mössbauer spectroscopy and using other results known from the literature.

2 Experimental

Glass containing 40 mol% Fe_2O_3 and 60 mol% P_2O_5 was prepared from high purity $NH_4H_2PO_4$ and Fe_2O_3. Approximately 20 mass% overweight of $NH_4H_2PO_4$ was used to compensate P_2O_5 losses during melting of the batch due to evaporation. The batch was melted for 2 h at 1373 K in an Al_2O_3 crucible in an electric furnace with the furnace atmosphere as close to natural as possible. The melt was vitrified by casting onto a steel plate and then crushed. The chemical composition of the obtained glass was checked by X-ray fluorescence spectroscopy and by X-ray diffraction to be amorphous.

Spectroscopic studies in the middle infrared (MIR) regions (4000–400 cm^{-1}) were carried out using a Fourier transform spectrometer Digilab FTS-60MVPC (Bio-Rad). The standard transmission technique was used. A sample of the glass was prepared as the standard KBr pellets and FITR spectra were collected after 256 scans with a resolution of 4 cm^{-1}.

Raman spectra of the glass have been collected using a FTS 6000 Bio-Rad Spectrometer with the Raman section (with Nd:YAG Spectra Physics T10, 1064 nm laser). Spectra were collected after 10 000 scans with a resolution of 4 cm^{-1}.

The X-ray absorption fine structure (XAFS) spectroscopy experiment was carried out at the BAMline beamline at a BESSY II storage ring in Berlin, Germany.[17] The measurements were performed in the transmission mode at the iron K-edge (7112 eV) using two 50 mm long ionization chambers (Oxford Danfysik IC Plus 50). The first chamber monitoring the incident beam intensity was filled with air, the second one detecting the absorption signal behind the sample was filled with argon, both at ambient pressure. This gave a transmittance of 0.9 for the first chamber and 0.25 for the second one in the energy range of interest. The energy was scanned using a Si(111) double crystal monochromator. The X-ray absorption near-edge structure (XANES) region was scanned with an energy step of 1 eV, whereas the extended X-ray absorption fine structure (EXAFS) was recorded with a constant step in the momentum space (k-space) of 0.05 Å^{-1} up to $k_{max} = 15$ Å^{-1} ($E_{max} = 7968$ eV). The acquisition time per point

19918 | *Phys. Chem. Chem. Phys.*, 2014, **16**, 19917–19927

This journal is © the Owner Societies 2014

was 4 s. The whole XAFS spectrum of the sample was recorded twice and averaged afterwards. The averaged spectrum underwent the standard procedure for obtaining the XAFS data using the Ifeffit (ver. 1.2.11c) software package.[18] The forward Fourier transform of the EXAFS part of the spectrum was performed applying a Hannig-type window in the range 2 to 9 Å^{-1} and a slope of d_k = 1.0. Such settings allowed for a good compromise between the maximum range of available data and the distortions induced by the noise stemming from data points with high k.

In the transmission XAFS experiment the studied glass was used as a thin powder sample with a layer thickness of 10 μm. The layer thickness d was chosen so that $\mu d \approx 1$, where μ is the linear absorption factor of the sample. This minimises the influence of the so called thickness effect[19] resulting from inhomogeneity of the layer, and causes damping of EXAFS oscillations. This in turn makes the evaluation of the coordination numbers unreliable. These, however, are one of the main parameters of interest of this XAFS study. The criterion chosen allows for a good balance between the negative impact of the thickness effect and a sufficient amount of absorbing material for a good signal-to-noise ratio.[20]

The ^{57}Fe Mössbauer spectroscopy studies were performed in transmission geometry at room temperature and at 77 K using a 25 mCi ^{57}Co γ-source embedded in the Rh matrix. The source was mounted onto a FAST Comtec Mössbauer drive unit working in constant velocity mode. Mössbauer transmission spectra were collected in a velocity range ±4 mm s^{-1} with 1024 channels before folding. The spectrometer was calibrated using standard α-Fe foil. The obtained spectra were deconvoluted with an application of two Voigt line shapes and Extended Voigt Based Fits (xVBF) were used to model distribution of iron sites in the amorphous glass.[21,22]

Density Functional Theory calculations at the B3LYP theory level were performed using Gaussian 09 D 0.1 software package.[23] For all calculations the same 6-311G(d) basis set was used. The composition of the computed clusters was close to stoichiometry of the synthesised basis glass. Geometry optimization was performed for all of the computed clusters and as a result theoretical FTIR and Raman spectra were calculated. Hydrogen atoms were used to terminate broken bonds at the model boundary.

3 Results

3.1 DFT simulations

Crystallization of 60P$_2$O$_5$–40Fe$_2$O$_3$ glass leads to the formation of two phases, namely α-FePO$_4$ and Fe$_2$P$_2$O$_7$, whose proportions strongly depend on the ratio of Fe^{3+}/Fe^{2+} ions.[16] Such glass structure should somehow reflect the particular crystallising phases. For a glass with only ferric iron crystallization of α-FePO$_4$ should be observed, which indeed is the main crystal phase in the case of the phosphate glasses with high Fe^{3+} content. The α-FePO$_4$ crystal structure, presented in Fig. 1, is composed of [FeO$_4$]$^-$ and [PO$_4$]$^+$ tetrahedra which share their vertices with each other and form even membered rings. In this structure every
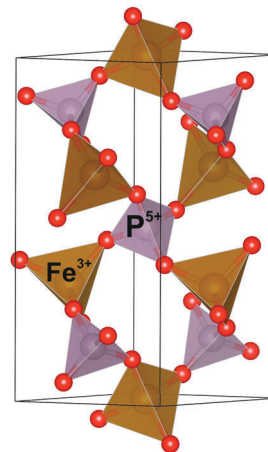

Fig. 1 Crystal structure of α-FePO$_4$.

P^{5+} cation is joined to four oxygen O^{2-} anions by a single bond. This leads to uncompensated charge +1 of [PO$_4$] tetrahedra. On the other hand iron is present as Fe^{3+} cations and forms [FeO$_4$]$^-$ tetrahedra. Thus an alternating arrangement of [PO$_4$]$^+$ and [FeO$_4$]$^-$ tetrahedra leads to charge neutrality of the crystal.

It is worth mentioning that an excess of 10 mol% of P$_2$O$_5$ exists in the studied glass. It can lead to the formation of similar even membered rings but smaller ones. This can result in breaking some of the P–O–Fe bonds and in the formation of P=O bonds and thus can lead to transformation of the structural units Q$_4$ to Q$_3$. Taking this into account, a fully optimized ring cluster (Fig. 2a) is proposed and for the purpose of further consideration it will be designated as the ring. The total energy per atom of the ring is −191.99 a.u. per at. Such rings can join each other and form the glass (Fig. 2b and c). The ratio of P/Fe in the ring is the same as the stoichiometry of the melt but there is a lack of one oxygen atom. This enhances reduction conditions of the melt and can reduce part of Fe^{3+} to Fe^{2+}. In the proposed ring the distance between two Fe ions is approximately 3.37 Å and it is comparable but smaller than
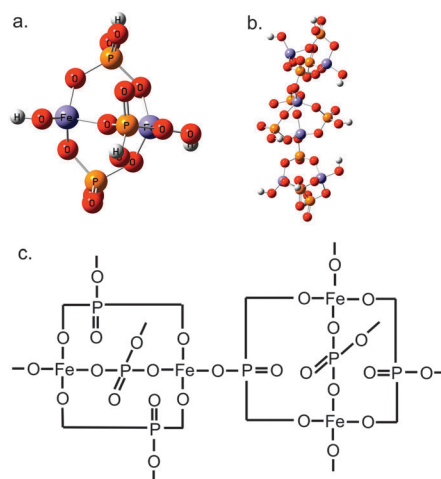

Fig. 2 Proposed and optimised ring (a), an exemplary connection of the rings (b), and a simplified scheme of the connection of two rings (c).
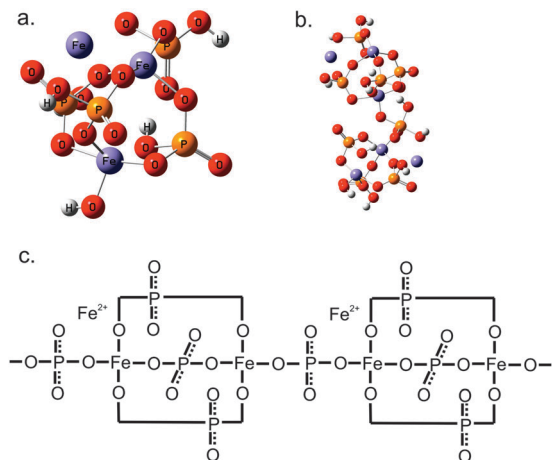
Fig. 3 Proposed and optimised unit of the $60P_2O_5$–$40Fe_2O_3$ glass (a), an exemplary connection of the units (b) and a simplified scheme of the connection of two units (c).

the experimental value 3.7 Å.[11,22] According to neutron diffraction studies[11] these two Fe ions should be aligned anti-parallel. Every Fe ion in the ring has the next Fe neighbour in the second ring at distances approximately 5.6 Å and 8.7 Å. The closer one should be coupled anti-parallel and the second one parallel,[11] which can lead to a magnetic frustration of the system. In the presented model the whole iron is in the Fe^{3+} state and forms $[FeO_4]^-$ tetrahedra with an unbalanced charge.

The reducing conditions of the melt change a part of ferric iron to ferrous, which can lead to breaking of some of the rings and changing the role of iron from a network former to a network modifier. The remnant P^{5+} and O^{2-} ions, which are left after decomposition of a part of the rings, can be joined to the remnant rings. The proposed new kind of structural unit of the glass after the optimization procedure is shown in Fig. 3a and for the purpose of further consideration it will be designated as the unit. The total energy of the unit is −247.55 a.u. per at and is lower than in the case of the ring. The stoichiometry of the unit is also close to the theoretical. The remnant P^{5+} and O^{2-} after decomposition of the ring are joined as new $[PO_4]$ tetrahedra to the $[FeO_4]$ tetrahedra. The rest of the oxygen anions leads to transformation of the structural units Q_3 to Q_2 which depolymerises the glass network. There are three different iron sites in the unit. Two sites in which iron is the glass network former: one in distorted tetrahedral coordination and the second one, where in the closest shell there is four oxygen atoms at a distance of about 1.86 Å and one at about 2.0 Å. The third Fe^{2+} ion plays the role of a network modifier and can be bonded to non-bridging oxygen of $[PO_4]$ tetrahedra. It is worth mentioning that this Fe^{2+} ion can also cross-link with the units that may increase the chemical durability. The units can be bonded with each other and they form a chain like structure as presented in Fig. 3b and c. The distance between Fe ions in the ring is approximately 3.66 Å. The distances between Fe ions in the next unit are 5.45 Å and 7.49 Å. These values are comparable with the experimental peaks observed in the magnetic correlation function.[11] The average P–O_{nb} (non-bridging oxygen)

distance is 1.47 Å and the P–O_b (bridging oxygen) distance is about 1.61 Å. Similar values and differences between them were previously observed experimentally[11,24,25] and also were simulated using classical molecular dynamics.[26] Moreover, Hoppe et al.[25] obtained experimentally P–O_{nb} and P–O_b distances equal to 1.46 Å and 1.62 Å respectively in Q_2 units, which are mostly observed in the simulated cluster. The neutron real space correlation function is characteristic of three peaks i.e. P–O, Fe–O and O–O at 1.50–1.55 Å, 1.89–1.93 Å and 2.47–2.51 Å, respectively[24,25,27] Similar mean lengths obtained according to the calculations are 1.57 Å, 1.90 Å and 2.49 Å, respectively.

Natural Bond Orbital (NBO)[28] analysis implemented in the Gaussian code was used to calculate the natural ionicity of a bond, as defined in ref. 29. The natural ionicity is zero for pure covalent bonds and can achieve any value between 0 and 1 for a pure ionic bond. The natural ionicity was lowest for the P–O bond (0.611) which as expected is more covalent than the Fe^{3+}–O bond (0.709) and Fe^{2+}–O bond (0.823) which are the most ionic in nature.

3.2 Raman spectroscopy

Raman spectroscopy has been widely used as an effective tool to study structural aspects of phosphate crystals and glasses. The frequency of the stretching vibrations of P–O bonds changes with the number of bridging oxygen atoms. The proper association of the measured peaks with the different P–O vibrational modes can be used to estimate structural elements of the studied glasses. This is especially important in the case of iron-phosphate glasses, in which because of high concentration of iron the NMR method could not be successfully used to determine the type and quantity of different phosphorous structural units.

The experimental Raman spectrum of the $60P_2O_5$–$40Fe_2O_3$ glass in the frequency region 200–2000 cm^{-1} is presented in Fig. 4. The first low frequency peak appears at about 350 cm^{-1} and is related to bending vibrations of PO_4 units with a cation as the modifier.[30] Overlapping of bending and torsional vibrations of iron oxygen polyhedral and pyrophosphate groups $(P_2O_7)^{4-}$ can be observed at 525 cm^{-1}.[31–34] The peaks below 600 cm^{-1} are in general related to different network bending modes. The peak in the range from 700 to 800 cm^{-1} is due to P–O–P symmetric
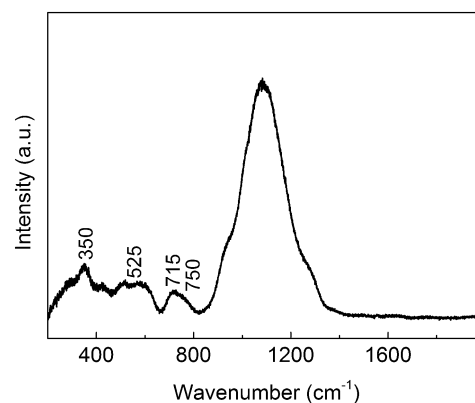

Fig. 4 The collected Raman spectrum of the $60P_2O_5$–$40Fe_2O_3$ glass.

19920 | *Phys. Chem. Chem. Phys.*, 2014, **16**, 19917–19927

This journal is © the Owner Societies 2014

Fig. 5 The experimental and the calculated Raman spectra of the $60P_2O_5–40Fe_2O_3$ glass.
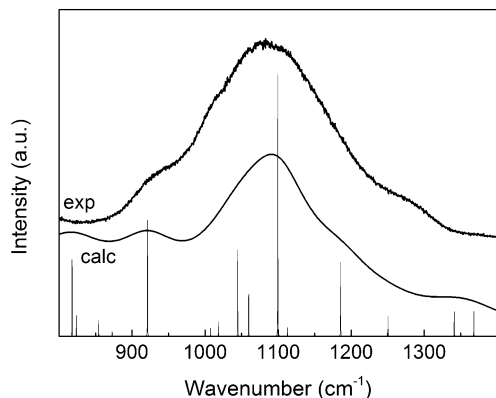

Fig. 6 The experimental and the calculated FTIR spectra of the $60P_2O_5–40Fe_2O_3$ glass.

stretch vibrations of Q^2 and Q^1 units. This peak is a convolution of two peaks *i.e.* one centred at about 715 cm^{-1} and the next centred at 750 cm^{-1}.[31–34] The first one can be assigned to vibrations of the two joined Q^2 units and the second one to those of Q^1 units.

At higher frequencies a large and asymmetric peak consisting of two smaller and strongly convoluted Gaussian lines can be observed. The experimental spectra in the narrower range of 850–1350 cm^{-1} is presented in Fig. 5.

Additionally, Fig. 5 presents the calculated Raman spectrum of the $60P_2O_5–40Fe_2O_3$ glass, determined assuming the proposed unit. The calculated spectrum was scaled by a scaling factor of 0.96[35] and the same peak half width at the half height of 40 cm^{-1} was used. From Fig. 5, it is evident that the experiment and the simulation are in a very good agreement. The simulation allowed to identify, assign and describe the main features of the spectra. The bands at about 920 cm^{-1} and 1050 cm^{-1} can be ascribed to symmetric and asymmetric stretching vibrations of Fe–O–P bonds, respectively. The highest Raman activity was observed at 1100 cm^{-1} and lower for higher frequencies at about 1200 cm^{-1} can be identified as symmetric and asymmetric vibrations of Q^2 units.

Some similarity between the $60P_2O_5–40Fe_2O_3$ glass and a quartz like compound α-FePO$_4$, can also be observed. This indicates that the crystal structure of this compound, based on tetrahedral [PO$_4$] and [FeO$_4$] units, is much closer to the glass structure than the orthorhombic form of FePO$_4$, based on [PO$_4$] tetrahedra and [FeO$_6$] octahedral units,[30] which additionally supports the proposed model.

3.3 Infrared spectroscopy

The experimental FTIR spectrum of $60P_2O_5–40Fe_2O_3$ glass in the frequency range 400–1500 cm^{-1} is presented in Fig. 6. The obtained spectrum is typical for iron phosphate glasses with the largest broad intensity band at 1000–1300 cm^{-1}. The spectrum is a convolution of many overlapping Gaussian components and a clear extraction of the particular components in this case is rather difficult.

For the proposed unit, a theoretical FTIR spectrum was also calculated and compared with its experimental counterpart (Fig. 6).
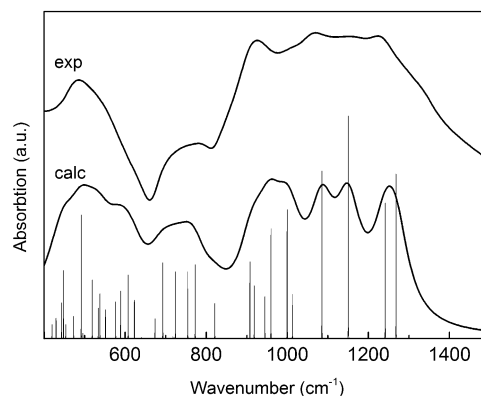
The spectrum was scaled using the same scaling factor and the same peak half width which was used in the case of the Raman measurement. From Fig. 6, it can be clearly seen that a very good agreement was achieved between the experiment and the simulation. The comparison of both experimental and simulated spectra allowed for assigning and describing the main features of the spectra. The collected spectrum is a convolution of many different vibrations and it can be divided into five characteristic regions. The first region in the wavenumber range of 500–600 cm^{-1} originates from the bending vibrations of Fe–O–P bonds. Then at higher frequencies of about 700–800 cm^{-1} and 900–1000 cm^{-1} symmetric and asymmetric vibrations of the Fe–O–P rings are evidenced, respectively. The next region of 1080–1150 cm^{-1} can be ascribed to stretching vibrations of bridging oxygen atoms in the Q_2 units and the last region at approximately 1250 cm^{-1} can be identified as stretching vibrations of P=O bonds in the Q_2 units.

3.4 Mössbauer spectroscopy

Mössbauer spectroscopy is a very powerful experimental method for investigating the oxidation state of iron atoms and their local environment. It is also sensitive to fine changes of their local environment caused by the first and even second neighbours of tested iron atoms. In the case of amorphous materials like glasses, the interpretation of a Mössbauer spectra is not so unambiguous like for crystalline compounds. In crystalline compounds every crystallographic iron site could be observed as one component of the spectrum. In disordered amorphous materials there are many different local iron environments and every one of them is described by a different set of hyperfine interaction parameters. As a consequence, the collected spectrum is a composition of many individual components. In oxide glasses every iron cation has only oxygen anions in the first neighbourhood, but deviations in coordination or iron–oxygen distance *etc.* should reflect the observed effect and the hyperfine interaction parameters. In the case of amorphous materials, one method for processing the spectra is an extended Voigtian based analysis (xVBF), which was described in detail elsewhere.[21,22] In this method every iron atom site is given by Gaussian distribution of the independent isomer shift
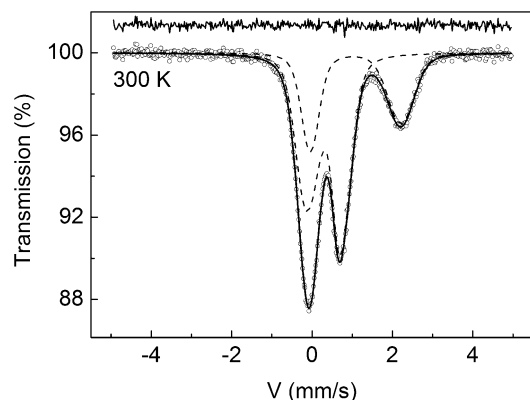
Fig. 7 ^{57}Fe transmission Mössbauer spectrum of the $60P_2O_5-40Fe_2O_3$ glass at 300 K.

and quadrupole splitting due to some randomness in the local environment of iron.

The ^{57}Fe transmission Mössbauer spectra collected at 300 K and 77 K are presented in Fig. 7 and 8, respectively.

The obtained spectra are typical for iron-phosphate glasses.[36] In Fig. 7 and 8 the coexistence of ferric and ferrous iron in the glass can be clearly observed. Both spectra were fitted assuming two different iron sites, namely one ferric and one ferrous site. In order to obtain a reasonable fit, the ferric component was modelled using two Gaussian distributions of the isomer shift. The probabilities of both distributions were set to 0.5 each and fixed during the fitting procedure. In this way, three different iron positions in the proposed glass unit could be distinguished *i.e.* one ferrous and one ferric, in which iron cations can be equally distributed among two different sites in the ring. As a consequence of the proposed fitting procedure, a very high consistency was obtained between the experimental Mössbauer spectra and the resulting fits, with a goodness parameter $\chi^2 = 1.00$ for both spectra collected at 295 K and 77 K. Fig. 7 and 8 also show differential patterns between the fits and the experimental points. The hyperfine interaction parameters for the $60P_2O_5-40Fe_2O_3$ glass at 300 K and 77 K are presented in Table 1, namely: A – area of the site, Pp – probability of the component,

Table 1 The hyperfine interaction parameters of $60P_2O_5-40Fe_2O_3$ glass at 300 K and 77 K

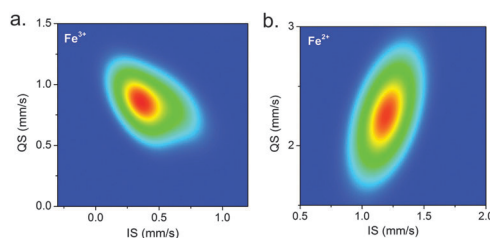| No.	A (%)	Pp (%)	IS (mm s^{-1})	σ_{IS} (mm s^{-1})	QS (mm s^{-1})	σ_{QS} (mm s^{-1})	r(IS,QS)
300 K							
1	66.1	0.5	0.326(10)	0.141(10)	0.846(10)	0.201(10)	−0.510
		0.5	0.541(10)	0.203(10)			
2	33.9	1.0	1.108(8)	0.173(8)	2.256(20)	0.335(20)	0.460
77 K							
1	63.5	0.5	0.442(5)	0.044(5)	0.737(5)	0.219(5)	0.296
		0.5	0.636(5)	0.091(5)			
2	36.5	1.0	1.205(4)	0.182(4)	2.654(9)	0.299(9)	0.615

Fig. 9 Contour map of the probability distribution of Fe^{3+} (a) and Fe^{2+} (b) ions as a function of IS and QS at 300 K.
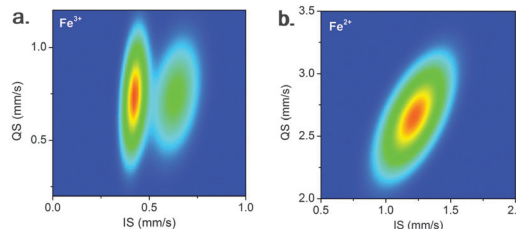

Fig. 10 Contour map of the probability distribution of Fe^{3+} (a) and Fe^{2+} (b) ions as a function of IS and QS at 77 K.

IS – isomer shift, QS – quadrupole splitting, σ_{IS} and σ_{QS} – Gaussian widths of the distribution of the isomer shift and quadruple splitting, respectively and r(IS,QS) – correlation parameter between IS and QS.

Fig. 9 and 10 present contour maps of the probability distributions of Fe^{3+} and Fe^{2+} cations as a function of IS and QS at 300 K and 77 K, respectively. Iron was introduced into the melt only in the Fe^{3+} form, but in the tested glass approximately 34% of iron is present as Fe^{2+} ions (Table 1, component 2). For other phosphate minerals, the isomer shift of Fe^{2+} cations in the octahedral and distorted bipyramidal coordination lies in the range of 1.15–1.27 mm s^{-1} and 1.10–1.16 mm s^{-1}, respectively.[35] The probability distribution of Fe^{2+} has the IS mean value of 1.108 mm s^{-1} at 300 K, which suggests that most of the Fe^{2+} ions are present in the distorted bipyramidal coordination. The value of IS for Fe^{2+} in phosphates also strongly depends on the Fe–O bond distance. According to ref. 37 and the obtained IS value, the mean Fe^{2+}–O distance can be estimated as 2.0 Å and is comparable to 2.1 Å estimated by Hoppe *et al.*[38] in similar glasses. On the other hand, the distribution is wide
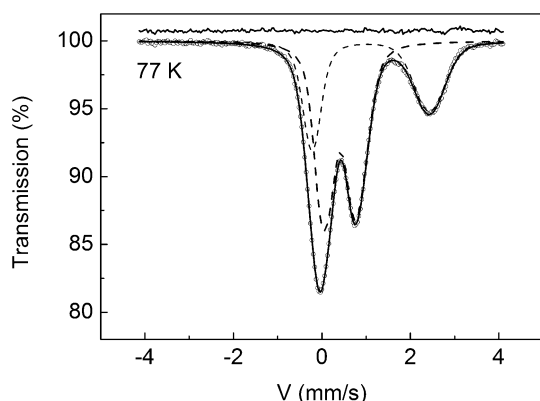

Fig. 8 ^{57}Fe transmission Mössbauer spectrum of the $60P_2O_5-40Fe_2O_3$ glass at 77 K.

19922 | *Phys. Chem. Chem. Phys.*, 2014, **16**, 19917–19927

This journal is © the Owner Societies 2014

σ_{QS} = 0.335 mm s^{-1} (Fig. 9b), which indicates that a part of the iron Fe^{2+} cations is present also in the octahedral coordination. The existence of Fe^{2+} in six- and five-fold coordination was confirmed previously by a neutron diffraction study.[24]

About 66% of iron in the investigated glass occurs in the Fe^{3+} form. According to the proposed structure of the glass, there are two different iron sites in the ring. One tetrahedral coordinated and one in fivefold coordination. These two sites are equally populated which was assumed during the fitting procedure by fixing probabilities of two IS Gaussian components. The value of IS differs significantly for these two components. The lower IS is about 0.326 mm s^{-1} at 300 K which in the experimental error range is close to the value 0.31 mm s^{-1}, which was previously reported for tetrahedral coordinated iron embedded in α-$FePO_4$.[39] The higher IS component can be assigned to iron in a higher coordination like fivefold, which is predicted by the proposed model. It is also worth mentioning that the distribution of $^{IV}Fe^{3+}$ hyperfine interaction parameters is narrower than the distribution of $^{V}Fe^{3+}$, which suggests a higher order of the tetrahedral Fe^{3+} surroundings. On the other hand, a relatively high value of QS for this site indicates a strong distortion thereof.

The mean value of the isomer shift of Fe^{3+} iron at 300 K is 0.433 mm s^{-1}. By comparison to silicate glasses, it is often related to octahedral or distorted octahedral coordination but it should be also noted that the mean values of the isomer shifts in phosphate minerals are higher than in the case of silicate minerals, although the Fe–O mean bond lengths are similar. This can be explained by a different covalence of the Si–O and the P–O bonds. The Si–O bonds in silicate minerals are more ionic than P–O bonds. This leads to a more covalent character of the bond in phosphates and thus oxygen atoms are more effective in withdrawing s-electron density from iron nuclei, which results in higher values of the isomer shift.

The hyperfine interaction parameters obtained for the 60P_2O_5–40Fe_2O_3 glass at 77 K are similar to those at 300 K. The values of IS at low temperature are higher, which is expected taking into account the second-order Doppler shift. The difference between isomer shifts IS values at 77 K and 300 K is approximately 0.1 mm s^{-1} and it is almost constant. This value is close to the value obtained previously for comparable iron-phosphate glasses.[40] It is also worth mentioning that the difference between Gaussian components at iron site 1 (Table 1) is about 0.2 mm s^{-1} and is temperature independent. In the similar way, the QS values measured at low temperature are higher. The difference of QS in the case of Fe^{3+} and Fe^{2+} sites is also in agreement with literature.[39] The distribution of hyperfine interaction parameters for Fe^{2+} ions (Fig. 9b and 10b) is almost the same, and at low temperature this distribution is a little bit narrower. The biggest difference is observed in distribution of the hyperfine parameters for Fe^{3+} ions (Fig. 9a and 10a). The lower temperature distribution is also narrower and the existence of two iron sites is easily resolved.

The similarity between the hyperfine interaction parameters obtained at two different temperatures can be a confirmation of stability of the proposed solution.

3.5 EXAFS/XANES

The background subtracted EXAFS spectrum of the 60P_2O_5–40Fe_2O_3 glass in the k-space is presented in Fig. 11a. It shows only one major frequency in the oscillation pattern, which is characteristic of amorphous materials.[41] This owes to the fact that the EXAFS is an interference effect and due to the random character of the atomic structure in glass only the nearest neighbours can contribute significantly to the constructive interference. The Fourier transformed EXAFS function, presented in Fig. 11b, shows that besides the major contribution from the nearest neighbours, some signals do come from the farther shells, but it is significantly weaker due to the disorder. For distances beyond 4.5 Å no signal is present. Thus, the only significant signal comes from the first coordination shell.

In order to interpret the EXAFS data quantitatively an analysis employing calculations using the FEFF 9 code[42] was carried out. Based on structural data available for this type of glass[24,43] a quick first shell theory model has been established. The model has a variable N-fold coordination symmetry with a Fe–O distance of 1.96 Å. The fit is carried out in the real part of the R-space using k_w = 1, 2, 3. The free parameters are: Debye–Waller factor (σ^2), inner core potential correction (ΔE_0), mean bond length distortion (Δr) and coordination number (N). The amplitude reduction factor (S_0^2), taking care of the EXAFS signal damping due to multiple-body effects during the absorption process, was set to 0.69, based on the analysis of pure metallic Fe standards. The fit gives the following results: N = 3.69(8), σ^2 = 0.0056(5) Å^2, Δr = −0.015(3) Å, and ΔE_0 = 2.64(19) eV. The correlation factor of the fit is R = 0.00165. The results of the quick first shell theory for these EXAFS data suggest that the Fe centres have on average a significantly lower coordination number than 6, and that on average the oxygen atoms are closer to the Fe ions. The mean length of the Fe–O bonds is 1.94(3) Å.

These findings seem to support the DFT model for the studied glass. And indeed when using this cluster for the calculation of EXAFS functions with FEFF 9, and performing a subsequent fit of the calculated EXAFS functions to the experimental data, an excellent agreement is achieved, *cf.* Fig. 11. The fit is carried out directly in the k-space. The fitting range is 2 Å^{-1} to 9 Å^{-1} with k_w = 1, 2, and 3 including only single scattering paths up to 3.3 Å. The calculations of the simulated EXAFS spectrum have to be performed on all three Fe centres of the DFT model, which for the purpose of the EXAFS study are labelled: Fe1, Fe2 (iron atoms in the ring) and Fe3. The proper superposition of the calculated
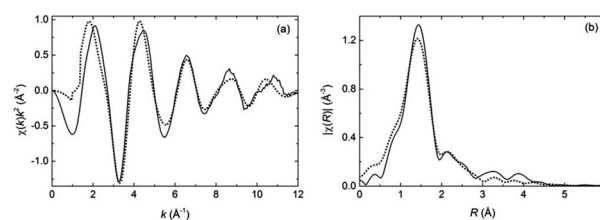

Fig. 11 (a) Experimental EXAFS spectrum in k-space (solid) and the calculated spectrum from the DFT model (dotted); (b) the corresponding Fourier transformed EXAFS curves in R-space.

This journal is © the Owner Societies 2014

Phys. Chem. Chem. Phys., 2014, **16**, 19917–19927 | **19923**

EXAFS curves is done by mathematical constraints in the fitting model. These are amongst others the abundances of each Fe site in the material, 0.35 for Fe1, 0.35 for Fe2 and 0.3 for Fe3. Due to the nature of the DFT model Fe3 is not suitable to be included in the fitting model, because it bridges two such clusters. Thus, it has an incomplete surrounding in the single chain model structure being used. Therefore, Fe2, which has a 5-fold symmetry, too, has to be taken instead. So the fraction of Fe2 is then 0.65. However, the Fe ion at the Fe3 site is divalent whereas the Fe ion at the Fe2 site is trivalent. Fe^{2+} is known to have in average longer Fe–O bonds by 0.2 Å than Fe^{3+}. This fact has to be taken into account when discussing the lattice distortion factor Δr for the Fe2 site. Furthermore, when one wants to combine two amplitudes of FEFF calculations via a fixed ratio, one has to keep in mind that FEFF assigns always an amplitude of 100 to the first scattering part. This has to be corrected by finding a scattering path to the same atom for each calculation. In this case these are Fe1–P2 and Fe2–P2, where P2 is atom no. 9 in the DFT model. These are scattering paths with an amplitude of 42.91 and an effective radius of 2.9925 Å for Fe1 and an amplitude of 43.05 and an effective radius of 2.6074 Å for Fe2. Assuming that the scattering amplitude is reversely proportional to the square of the scattering path radius, one can easily calculate the correction factor by which the two amplitudes of the FEFF calculations are related, by multiplying the ratios of the calculated scattering amplitudes, the squares of the respective path radii and the relative abundances, $43.05/42.91 \times (2.6074)^2/(2.9925)^2 \times 0.65/0.35 = 1.41$. This coefficient allows the use of only one free parameter for the amplitude (A) in the fitting model. The other fit parameters are: the Debye–Waller factor (σ^2) and the bond length distortion (Δr) for each Fe site and one inner core potential correction factor (ΔE_0) for the whole fitting model. These are in total 6 free fit parameters. The results of the fitting procedure are presented in Table 2.

As expected the Δr parameter for the Fe2 site is significantly larger than for the Fe1 site, because it contains also the correction for the 5-fold coordinated Fe^{2+} ion placed in the Fe3 site. If one assumes that the lattice distortion at the 5-fold coordinated Fe^{3+} ion placed in the Fe2 site is of the same order as that for the 4-fold coordinated Fe^{3+} ion placed in the Fe1 site, one gets estimated values for the mean bond length elongation at the Fe3 site, 5-fold coordinated Fe(ii), $\Delta r = 0.282$ Å; a value expected for the bond length difference between divalent and trivalent ions. In general the mean distance of all Fe–O bonds in the fitted model amounts to 1.94 Å, which is in agreement with the quick first shell theory.

The DFT model was used for the calculation of a XANES spectrum in order to reproduce the experimental one. The XANES spectrum is very sensitive to small changes in the local symmetry, as reported elsewhere.[44] Additionally, calculations of the XANES spectra using the FEFF 9 code do not take any free parameters and use a full-multiple scattering algorithm rather than a simple path expansion as in the case of EXAFS calculations. Therefore, this is a good probe for the verification of the fit results obtained from the EXAFS analysis and the structural model in general. Like in the case of EXAFS calculations, separate calculations of the theoretical XANES spectra are done at each Fe site of the cluster. Due to the very same reasons as for the EXAFS case the Fe2 site (5-fold coordinated Fe^{3+}) and the Fe3 site (5-fold coordinated Fe^{2+}) are combined and represented by one calculation. A superposition of two calculations combined by the same coefficient as for the EXAFS case is then representing the calculated XANES curve, as presented in Fig. 12. As one can see that the curve reproduces all significant spectral features of the experimental spectra, despite the fact in the simulations the larger interatomic distance at the 5-fold coordinated Fe^{2+} site was not taken into account. This and the EXAFS analysis show that the DFT model is representative of the local structure of the investigated $60P_2O_5–40Fe_2O_3$ glass.

4 Discussion

The conducted DFT simulations and structural studies of the $60P_2O_5–40Fe_2O_3$ glass allowed us to propose a structural model of the glass. The starting point in presented considerations was the α-FePO$_4$ crystal structure which is built of $[PO_4]^+[FeO_4]^-$ tetrahedra joined and sharing common vertices. The $[PO_4]^+$ has an unbalanced charge +1 but on the other side $[FeO_4]^-$ has a charge −1, so both of them compensate their charges and there are no P=O double bonds. In this case only Q_4 units exist. The $[PO_4][FeO_4]$ tetrahedra form even membered rings and alternate each other. Increasing P_2O_5 content results in the formation of smaller rings, as proposed in Fig. 2a, and in the case of the studied glass the structure could be built only using them to maintain the desired stoichiometry of the melt. There is enough oxygen to transform one of the Q_4 units to the Q_3 unit, which leads to a small unbalanced charge on $[FeO_4]$. The increasing oxygen concentration in the melt increases the tendency for further transformation of Q_4 to Q_3 and even to Q_2 units, which changes the glass structure from a three dimensional cross-linked network to polymer like chains. In this case the charge of $[FeO_4]$ tetrahedra is fully unbalanced. These rings join together and can build the glass, as shown in Fig. 2b. The reducing conditions during the synthesis of the glass reduce a part of Fe^{3+} ions to Fe^{2+} ions, which is observed as

Table 2 Best fit parameter values and the correlation factor of the EXAFS analysis using the DFT model

	A	σ^2 (Å^2)	Δr (Å)	ΔE_0 (eV)	R
Fe1–Fe(iii) 4-fold coordinated	0.38(4)	0.001(2)	0.018(9)	7.2(9)	0.052
Fe2–Fe(ii) and Fe(iii) 5-fold coordinated	0.55^a	0.009(4)	0.14(2)		

^{a} A_{Fe2} value not fitted, but connected to A_{Fe1} by the relation $A_{Fe2} = 1.41A_{Fe1}$ (see text).

19924 | *Phys. Chem. Chem. Phys.*, 2014, **16**, 19917–19927

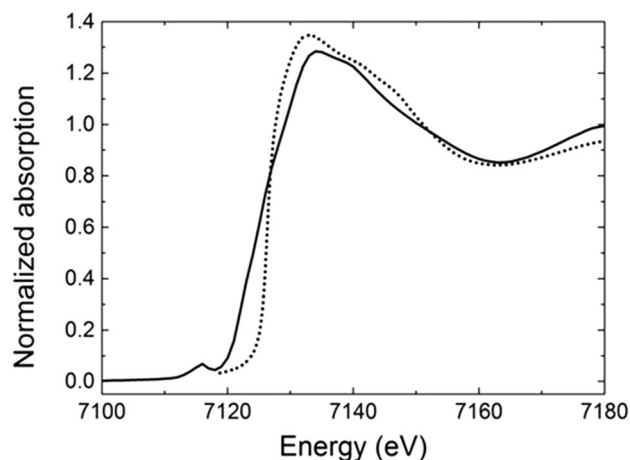This journal is © the Owner Societies 2014

Fig. 12 The experimental XANES spectrum (solid) and the calculated spectrum (dotted) based on the DFT model cluster.

the disintegration of some rings and results in the formation of the units shown in Fig. 3a. In this case the melt is richer in oxygen and all Q_4 units are transformed to Q_3 and Q_2 depending on the Fe^{2+} ion concentration, which changes the glass network from a three dimensional cross-linked network to a chain-like structure. Thus, iron is changing its role from a glass structure former to a glass modifier. In the proposed glass unit Fe^{2+} ions can behave as a typical glass network modifier joined to non-bridging oxygen atoms and cross-link glass chains, which can increase the stability of the glass structure or can be a charge compensator of $[FeO_4]^-$ tetrahedra in the rings. To fully compensate the unbalanced $[FeO_4]^-$ tetrahedra at least approximately 33% of iron atoms should be reduced from Fe^{3+} to Fe^{2+}, as in the case of the synthesized glass. It is worth mentioning that the total energy per atom of the unit is lower than the energy of the ring, which suggests that the unit is more preferable and additionally enhances the reduction of iron.

Previous investigations of the same base glass but loaded with caesium revealed that in the obtained glasses there were almost only Fe^{3+} ions.[14,15] It is interesting that no special structural changes were observed with increasing Cs_2O content in the base glass up to 22 mol%. Further increase of the caesium content elicits rebuilding of the glass structure.[15] The transformation and melting temperatures both rise with increasing Cs_2O content up to 22 mol% and above this value they are reduced. The increase of these temperatures is unusual and cannot be explained assuming Cs as a typical glass structure modifier.

Due to the lack of Fe^{2+} ions, the structure of these glasses can also be described by the proposed rings. In this case the Cs^+ ion can be a charge compensator for the $[FeO_4]^-$ which strongly bonds them. Moreover, one O^{2-} anion introduced by Cs_2O changes the Q_4 to Q_3 units. Thus one ring needs two Cs^+ ions to fully compensate its charge and to get one O^{2-} anion which transforms two Q_4 to Q_3 units. In this case the glass is built only of Q_3 units. The situation in which one Cs_2O particle falls in one ring corresponds to exactly 22 mol% concentration of Cs_2O in the glass. The charge balancing role of Cs^+ stabilises the rings, fills the voids in the glass, increases its density as reported[14,15] and makes the structure more rigid, which results in an increase of both transformation and melting

temperatures. A further increase of the Cs_2O content leads to breaking of Fe–O–P bonds and shortening of the chains, which can be observed as the rebuilding of the glass structure. The structural change makes the structure more flexible, which causes a reduction of the above-mentioned temperatures.

Similar results like for Cs_2O were previously observed in studies over the immobilization of Na_2SO_4, but the rebuilding of the structure was suggested if Na_2O concentration in the glass exceeds about 30 mol%.[16] In these studies the base glass was synthesised under the same conditions as in this paper, which let us assume a similar content of Fe^{2+} cations like in the investigated $60P_2O_5$–$40Fe_2O_3$ glass. If all of the Fe^{2+} cations act as glass modifiers and can cross-link the chains built of the proposed units, then two Na^+ cations are required in the ring in order to fully compensate the charge of the $[FeO_4]^-$, and one O^{2-} anion transforms two Q_3 units to Q_2. There is still a possibility of joining one Q_3 unit with one Na^+ cation. The higher concentration of Na_2O causes the chains built of the structural units to break and separate themselves, which can be observed as the rebuilding of the glass structure. Thus the proposed structural unit is able to join about $1.5Na_2O$ particles per unit without complete separation of the glass chain, which gives approximately 30 mol% of Na_2O.

According to the obtained results of natural ionicity the most covalent bond is the P–O bond, which makes it rigid, leading to the formation of little distorted tetrahedra. On the other hand, the Fe^{3+}–O bond is much more ionic in its nature, thus more flexible. Therefore the $[FeO_4]$ tetrahedra can be much more distorted and the glass network can bend on them in order to accommodate different elements. The iron-phosphate glasses belong to the group of magnetic oxide glasses in which magnetic moments are spatially distributed in a disordered fashion like spin glass. The magnetic structure of these glasses is quite complex and confirms the presence of speromagnetic ordering.[11–13] The magnetic correlation function obtained by the neutron scattering method shows the existence of negative peaks at 3.7 Å and 5.8–5.9 Å. This suggests that the average magnetic moment of the atoms at these distances tends to be anti-parallel and the broad positive effect at 8–10 Å distance.[10] The $60P_2O_5$–$40Fe_2O_3$ glasses[11] are similar to the glass studied in this paper. Therefore, the same structural model built of the units which are joined in long chains, can be applied. The distance between two iron atoms in the unit is 3.66 Å and the magnetic moments of these iron atoms are coupled antiferromagnetically, as expected. Every iron atom in the ring has the next iron atoms at a distance 5.45 Å and 7.49 Å from the next structural unit in the chain. If the magnetic moments of the atoms at the 5.45 Å distance are anti-parallel, the magnetic moments of the atoms at a further distance of 7.49 Å will have to be parallel to maintain anti-parallel coupling of the magnetic moments in the ring. This explains the magnetic structure of the iron-phosphate glasses.

5 Conclusions

A structural model of the $60P_2O_5$–$40Fe_2O_3$ glass is proposed, according to which, the glass is built of two kinds of structural units depending on the Fe^{3+}/Fe^{2+} ratio. The starting point of the

This journal is © the Owner Societies 2014

Phys. Chem. Chem. Phys., 2014, **16**, 19917–19927 | **19925**

model is the crystal structure of α-$FePO_4$, which is the main crystal phase in the case of iron-phosphate glasses with high Fe^{3+} content. The presented model anticipates three iron sites *i.e.* one site for Fe^{2+}, which can be highly distorted with mean coordination number 5, and two sites for Fe^{3+}, which are part of the rings. In these sites iron is placed in tetrahedral coordination, but higher coordination like 5 is also possible. Thus the glass, depending on the Fe^{2+} concentration, can be built of α-$FePO_4$-like regions. The obtained Fe^{3+}–O bond ionicity is lower than the Fe^{2+}–O, but considerably higher than that of P^{5+}–O. This makes the Fe^{3+}–O bonds more flexible than the P^{5+}–O bonds, which leads to a higher distortion of the $[FeO_4]$ tetrahedra than of $[PO_4]$. On the other hand, an increase of the glass network flexibility conduces to much easier accommodation of waste constituents, leading to a high waste loading possibility of the glass.

According to the model, alkali metals function as charge compensators up to 20–30% mol concentration and are strongly bonded to the glass. This manifests itself as chemical durability of the glass and an increase of the glass transformation temperature in this region.

Moreover, the presented model can also explain the complicated magnetic structure of the studied glass. Finally, it is worth mentioning that the proposed theoretical considerations are in very good agreement with the structural studies presented in this work.

Acknowledgements

References

1 I. W. Donald, *Glass Technol.*, 2007, **48**, 155–163.

2 I. Ojovan, W. Lee and W. Lee, *An Introduction to Nuclear Waste Immobilisation*, Elsevier Science, 2010.

3 I. Wacawska and M. Szumera, *J. Therm. Anal. Calorim.*, 2010, **101**, 423–427.

4 R. K. Brow, *J. Non-Cryst. Solids*, 2000, **263–264**, 1–28.

5 C.-W. Kim and D. E. Day, *J. Non-Cryst. Solids*, 2003, **331**, 20–31.

6 P. A. Bingham, R. J. Hand and C. R. Scales, *Symposium Scientific Basis for Nuclear Waste Management XXIX*, 2006.

7 U. Hoppe, *J. Non-Cryst. Solids*, 1996, **195**, 138–147.

8 J. Shelby, *Introduction to Glass Science and Technology*, Royal Society of Chemistry, 2005.

9 F. Wedgwood and A. Wright, *J. Non-Cryst. Solids*, 1976, **21**, 95–105.

10 G. Marasinghe, M. Karabulut, C. Ray, D. Day, M. Shumsky, W. Yelon, C. Booth, P. Allen and D. Shuh, *J. Non-Cryst. Solids*, 1997, **222**, 144–152.

11 A. C. Wright, R. N. Sinclair, J. L. Shaw, R. Haworth, G. K. Marasinghe, D. E. Day, P. A. Bingham, S. D. Forder, G. J. Cuello and H. E. Fischer, *Phys. Chem. Glasses: Eur. J. Glass Sci. Technol., Part B*, 2012, **53**, 227–244.

12 J. L. Shaw, A. C. Wright, R. N. Sinclair, G. K. Marasinghe, D. Holland, M. R. Lees and C. R. Scales, *J. Non-Cryst. Solids*, 2004, **345–346**, 245–250.

13 H. Akamatsu, S. Oku, K. Fujita, S. Murai and K. Tanaka, *Phys. Rev. B: Condens. Matter Mater. Phys.*, 2009, **80**, 134408.

14 K. Joseph, M. Premila, G. Amarendra, K. G. Kutty, C. Sundar and P. V. Rao, *J. Nucl. Mater.*, 2012, **420**, 49–53.

15 K. Joseph, K. G. Kutty, P. Chandramohan and P. V. Rao, *J. Nucl. Mater.*, 2009, **384**, 262–267.

16 P. Stoch, M. Ciecinska and A. Stoch, *J. Therm. Anal. Calorim.*, 2014, **117**, 197–204.

17 H. Riesemeier, K. Ecker, W. Görner, B. Müller, M. Radtke and M. Krumrey, *X-Ray Spectrom.*, 2005, **34**, 160–163.

18 B. Ravel and M. Newville, *J. Synchrotron Radiat.*, 2005, **12**, 537–541.

19 S. M. Heald and E. A. Stern, *Phys. Rev. B: Solid State*, 1977, **16**, 5549–5559.

20 G. Bunker, *Introduction to XAFS: A Practical Guide to X-ray Absorption Fine Structure Spectroscopy*, Cambridge University Press, 2010.

21 C. Wivel and S. Morup, *J. Phys. E: Sci. Instrum.*, 1981, **14**, 605.

22 H. Alberto, J. P. da Cunha, B. Mysen, J. Gil and N. A. de Campos, *J. Non-Cryst. Solids*, 1996, **194**, 48–57.

23 M. J. Frisch, G. W. Trucks, H. B. Schlegel, G. E. Scuseria, M. A. Robb, J. R. Cheeseman, G. Scalmani, V. Barone, B. Mennucci, G. A. Petersson, H. Nakatsuji, M. Caricato, X. Li, H. P. Hratchian, A. F. Izmaylov, J. Bloino, G. Zheng, J. L. Sonnenberg, M. Hada, M. Ehara, K. Toyota, R. Fukuda, J. Hasegawa, M. Ishida, T. Nakajima, Y. Honda, O. Kitao, H. Nakai, T. Vreven, J. A. Montgomery Jr, J. E. Peralta, F. Ogliaro, M. Bearpark, J. J. Heyd, E. Brothers, K. N. Kudin, V. N. Staroverov, R. Kobayashi, J. Normand, K. Raghavachari, A. Rendell, J. C. Burant, S. S. Iyengar, J. Tomasi, M. Cossi, N. Rega, J. M. Millam, M. Klene, J. E. Knox, J. B. Cross, V. Bakken, C. Adamo, J. Jaramillo, R. Gomperts, R. E. Stratmann, O. Yazyev, A. J. Austin, R. Cammi, C. Pomelli, J. W. Ochterski, R. L. Martin, K. Morokuma, V. G. Zakrzewski, G. A. Voth, P. Salvador, J. J. Dannenberg, S. Dapprich, A. D. Daniels, Ö. Farkas, J. B. Foresman, J. V. Ortiz, J. Cioslowski and D. J. Fox, *Gaussian 09 Revision D.01*, Gaussian Inc., Wallingford CT, 2009.

24 A. C. Wright, R. N. Sinclair, J. L. Shaw, R. Haworth, G. K. Marasinghe and D. E. Day, *Phys. Chem. Glasses: Eur. J. Glass Sci. Technol., Part B*, 2008, **49**, 1–7.

25 U. Hoppe, G. Walter, R. Kranold and D. Stachel, *J. Non-Cryst. Solids*, 2000, **263–264**, 29–47.

26 B. Al-Hasni and G. Mountjoy, *J. Non-Cryst. Solids*, 2011, **357**, 2775–2779.

27 B. M. Al-Hasni, G. Mountjoy and E. Barney, *J. Non-Cryst. Solids*, 2013, **380**, 141–152.

28 J. P. Foster and F. Weinhold, *J. Am. Chem. Soc.*, 1980, **102**, 7211–7218.

19926 | *Phys. Chem. Chem. Phys.*, 2014, **16**, 19917–19927

This journal is © the Owner Societies 2014

29 F. Weinhold and C. R. Landis, *Discovering Chemistry with Natural Bond Orbitals*, John Wiley and Sons, Inc., 2012.

30 L. Zhang and R. K. Brow, *J. Am. Ceram. Soc.*, 2011, **94**, 3123–3130.

31 Y. Lai, X. Liang, S. Yang, J. Wang, L. Cao and B. Dai, *J. Mol. Struct.*, 2011, **992**, 84–88.

32 C. Kim, C. Ray, D. Zhu, D. Day, D. Gombert, A. Aloy, A. Mogu-Milankovi and M. Karabulut, *J. Nucl. Mater.*, 2003, **322**, 152–164.

33 C.-W. Kim and D. E. Day, *J. Non-Cryst. Solids*, 2003, **331**, 20–31.

34 T. Jermoumi, M. Hafid, N. Niegisch, M. Mennig, A. Sabir and N. Toreis, *Mater. Res. Bull.*, 2002, **37**, 49–57.

35 C. Cramer, *Essentials of Computational Chemistry: Theories and Models*, Wiley, 2005.

36 P. Stoch, M. Ciecinska, P. Zachariasz, J. Suwalski, L. Gorski and T. Wojcik, *Nukleonika*, 2013, **58**, 63–66.

37 I. Shino and Z. Li, *Am. Mineral.*, 1998, **83**, 1316–1322.

38 U. Hoppe, M. Karabulut, E. Metwalli, R. K. Brow and P. Jóvári, *J. Phys.: Condens. Matter*, 2003, **15**, 6143.

39 J. Millet, C. Virely, M. Forissier, P. Bussiére and J. Vedrine, *Hyperfine Interact.*, 1989, **46**, 619–628.

40 L. Aldon, A. Perea, M. Womes, C. Ionica-Bousquet and J.-C. Jumas, *J. Solid State Chem.*, 2010, **183**, 218–222.

41 H. Bertagnolli and T. S. Ertel, *Angew. Chem., Int. Ed. Engl.*, 1994, **33**, 45–66.

42 J. J. Rehr, J. J. Kas, F. D. Vila, M. P. Prange and K. Jorissen, *Phys. Chem. Chem. Phys.*, 2010, **12**, 5503–5513.

43 M. Karabulut, G. Marasinghe, C. Ray, D. Day, G. Waddill, C. Booth, P. Allen, J. Bucher, D. Caulder and D. Shuh, *J. Non-Cryst. Solids*, 2002, **306**, 182–192.

44 J. Rehr and A. Ankudinov, *Coord. Chem. Rev.*, 2005, **249**, 131–140.